

See discussions, stats, and author profiles for this publication at: <https://www.researchgate.net/publication/271533189>

# Optical Magnetism and Plasmonic Fano Resonances in Metal–Insulator–Metal Oligomers

ARTICLE *in* NANO LETTERS · JANUARY 2015

Impact Factor: 13.59 · DOI: 10.1021/nl504802r · Source: PubMed

---

CITATIONS

5

READS

211

## 4 AUTHORS, INCLUDING:



R. Verre

Chalmers University of Technology

22 PUBLICATIONS 81 CITATIONS

[SEE PROFILE](#)



Timur Shegai

Chalmers University of Technology

29 PUBLICATIONS 888 CITATIONS

[SEE PROFILE](#)



Mikael Käll

Chalmers University of Technology

50 PUBLICATIONS 1,199 CITATIONS

[SEE PROFILE](#)

# <sup>1</sup> Optical Magnetism and Plasmonic Fano Resonances in Metal–Insulator–Metal Oligomers

<sup>3</sup> R. Verre,\* Z. J. Yang, T. Shegai, and M. Käll\*

<sup>4</sup> Department of Applied Physics, Chalmers University of Technology, 41296 Göteborg, Sweden

<sup>5</sup> Supporting Information

**ABSTRACT:** The possibility of achieving optical magnetism at visible frequencies using plasmonic nanostructures has recently been a subject of great interest. The concept is based on designing structures that support plasmon modes with electron oscillation patterns that imitate current loops, that is, magnetic dipoles. However, the magnetic resonances are typically spectrally narrow, thereby limiting their applicability in, for example, metamaterial designs. We show that a significantly broader magnetic response can be realized in plasmonic pentamers constructed from metal–insulator–metal (MIM) sandwich particles. Each MIM unit acts as a magnetic meta-atom and the optical magnetism is rendered quasi-broadband through hybridization of the in-plane modes. We demonstrate that scattering spectra of individual MIM pentamers exhibit multiple Fano resonances and a broad subradiant spectral window that signal the magnetic interaction and a hierarchy of coupling effects in these intricate three-dimensional nanoparticle oligomers.

**KEYWORDS:** Plasmonic antennas, artificial magnetism, Fano resonances, metamaterials, dark-field scattering



<sup>22</sup> Light manipulation based on optical antennas and <sup>23</sup> metamaterials built from coupled plasmonic nanoparticles <sup>24</sup> is key to a wide spectrum of existing and proposed <sup>25</sup> nanophotonics applications, including plasmonic lasing,<sup>1</sup> single <sup>26</sup> molecule recognition,<sup>2</sup> solar light harvesting,<sup>3</sup> photocatalytic <sup>27</sup> enhancement,<sup>4</sup> and optoelectronics devices.<sup>5,6</sup> Many of these <sup>28</sup> applications utilize the fact that the interaction between <sup>29</sup> plasmonic particles in close proximity can be so strong that <sup>30</sup> the optical response of the composite system differs drastically <sup>31</sup> from that of the isolated constituents.<sup>7,8</sup> One such case is the <sup>32</sup> plasmonic nanosandwich, or metal–insulator–metal (MIM) <sup>33</sup> dimer, composed of two metal nanodisks separated by a thin <sup>34</sup> dielectric spacer.<sup>9</sup> For spacers with sufficiently small thickness, <sup>35</sup> the in-plane dipole resonances in the individual nanodisks <sup>36</sup> hybridize vertically such that two new eigenmodes appear, one <sup>37</sup> of which has the character of a circulating pseudocurrent, that <sup>38</sup> is, a magnetic dipole.<sup>10,11</sup> The MIM dimer is the simplest <sup>39</sup> structure that can generate “optical magnetism”, that is, artificial <sup>40</sup> magnetism at optical frequencies, although most work in this <sup>41</sup> field has focused on more complex nanostructures, like split <sup>42</sup> ring resonators,<sup>12,13</sup> various particle assemblies<sup>14–21</sup> and fishnet <sup>43</sup> materials.<sup>22</sup> Optical magnetism is a key ingredient in many <sup>44</sup> proposed metamaterials applications based on negative <sup>45</sup> refraction, including perfect lensing, as well as in electro- <sup>46</sup> magnetic cloaking.<sup>23</sup> However, most nanostructures investi- <sup>47</sup> gated so far, including the MIM dimer, suffers from the same <sup>48</sup> drawback, namely that optical magnetism only occurs in a <sup>49</sup> narrow spectral window centered on a single resonance <sup>50</sup> wavelength, thus severely limiting their practical applicability.

One way to broaden the spectral response of plasmonic <sup>51</sup> resonances without causing unwanted resistive losses, is to <sup>52</sup> group particles together into clusters that exhibit so-called <sup>53</sup> super-radiance. This phenomenon occurs when dipole <sup>54</sup> oscillations of neighboring particles oscillate in-phase such <sup>55</sup> that their scattered fields superpose constructively and <sup>56</sup> therefore generate strongly enhanced radiative damping.<sup>57</sup> Super-radiance and related effects have been intensively <sup>58</sup> explored in plasmonic particle oligomers, typically in the <sup>59</sup> form of two-dimensional (2D) centrosymmetric arrangements.<sup>60</sup> Scattering and extinction spectra from such structures usually <sup>61</sup> reveal a broad and intense super-radiant band but also a narrow <sup>62</sup> spectral “dip” with a characteristic asymmetric Fano <sup>63</sup> shape.<sup>20,24,25</sup> This spectral feature is caused by destructive, or <sup>64</sup> subradiant, interferences due to antiphase oscillations of <sup>65</sup> neighboring particle dipoles, which reduce the total dipole <sup>66</sup> moment of the oligomer. Nanoparticle oligomers have recently <sup>67</sup> attracted interest as nanophotonic building blocks in <sup>68</sup> applications like optical switching,<sup>26</sup> refractometric sensing,<sup>27</sup> <sup>69</sup> and nonlinear optics.<sup>28,29</sup> They can also exhibit optical <sup>70</sup> magnetism due to coil-type circulating current modes.<sup>30,31</sup> <sup>71</sup> However, the magnetic dipole moments associated with these <sup>72</sup> pseudocurrents are oriented perpendicular to the plane of the <sup>73</sup> oligomer and therefore only couple weakly to light that is <sup>74</sup> incident normal to the surface supporting the structure.<sup>75</sup>

**Received:** December 15, 2014

**Revised:** January 21, 2015

In this Letter, we explore the possibility to broaden the in-plane magnetic response of the MIM dimer through super-radiance in an oligomer structure, as illustrated schematically in Figure 1. We focus entirely on MIM pentamers with  $C_4$

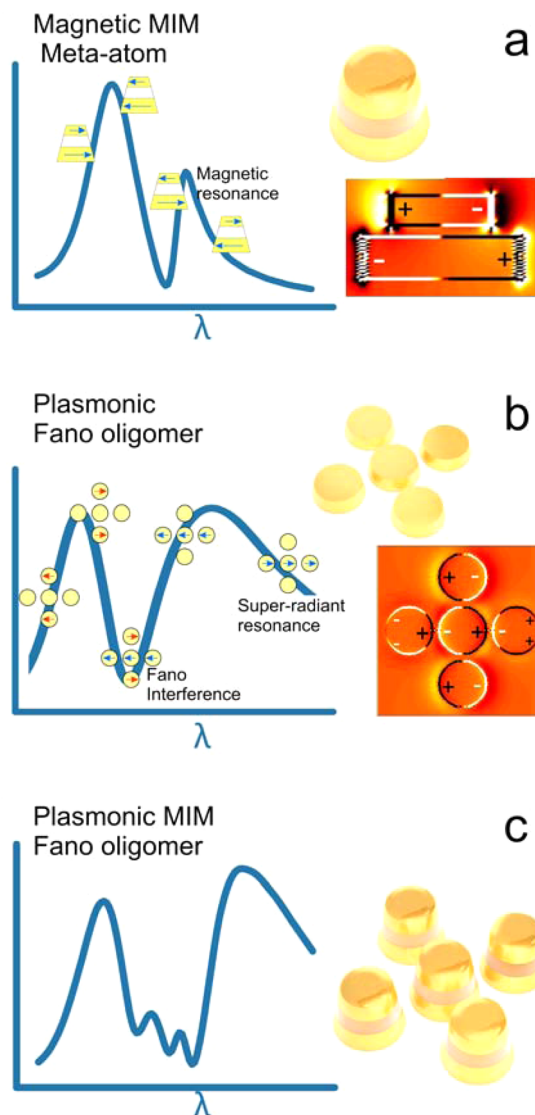


**Figure 1.** (a) Scattering properties of a vertical MIM dimer meta-atom. The structure presents an in-phase and an out-of-phase mode. The out-of-phase mode produces an in-plane magnetic field in the dielectric spacer due to the formation of coil-like currents. (b) Scattering properties of a plasmonic Fano pentamer. In this case, destructive interference between a super-radiant mode and a narrow mode produces dip with an asymmetric line shape. The simulated charge distributions at the magnetic resonance and at the Fano dip wavelength are shown as insets. (c) The combination of the two systems is a MIM oligomer that is expected to present a complex scattering behavior. The MIM pentamer supports multiple subradiant modes that generate a quasi-broadband magnetic response at visible frequencies.

symmetry, that is, four MIM dimers positioned symmetrically around a fifth dimer, because the structure is polarization insensitive. We show that a plethora of new spectral features arise in this complex coupled structure, which thus combines the vertical and in-plane interactions described above. In particular, we find an intriguing set of overlapping Fano

antiresonances that signal the appearance of optical magnetism over a significant part of the visible to near-infrared spectral range. These findings may contribute toward the development of metamaterials with a broadband magnetic response, as well as to the general understanding and applications of three-dimensional (3D) optical antenna structures with engineered radiative properties.

The MIM pentamers were made through a combination of electron beam lithography, evaporation, and lift-off. Each MIM dimer is composed of two gold nanodisks separated by an  $\text{Al}_2\text{O}_3$  dielectric spacer with thickness  $s = 10$  or 20 nm. For each spacer thickness, the in-plane edge-to-edge gap between the bottom disks,  $g$ , was varied between 80 and 20 nm. We also produced isolated MIM dimers and pentamers composed of homogeneous nanodisks for comparison. Figure 2a shows a SEM side view of one of the plasmonic MIM pentamers. Each dimer has a truncated conical shape and a clear contrast between the different materials is visible. The nomenclature used throughout the text is explained in Figure 2b. The diameters of the bottom ( $d_B$ ) and top ( $d_T$ ) disks were measured to be 130 and 85 nm, respectively. The heights ( $h_B$ ,  $h_T$ ) of the nanodisks were set to (35, 25 nm) and (40, 30 nm) for the  $s = 20$  nm and  $s = 10$  nm samples, respectively, means that the total dimer height is 80 nm for all structures. The optical properties of the MIM pentamers were analyzed one-by-one using dark-field scattering of unpolarized light measured in an inverted optical microscope. Figure 2c shows representative spectra together with SEM images and calculated scattering spectra obtained through finite-difference time-domain (FDTD) simulations, see the Supporting Information for complete details on the experiments and simulations.

The size parameters of the MIM dimers were chosen such that the diameter:height aspect ratio of the individual nanodisks was approximately constant and such that the most prominent spectral features occurred in the visible/NIR range. The similar nanodisk aspect ratios result in similar dipolar plasmon resonance wavelengths and therefore strong plasmon hybridization within and between the MIM dimers. Scattering spectra from isolated MIM dimers are shown in the first row of Figure 2c. As expected, and as illustrated in Figure 1a, one observes two hybridized resonances: a high energy mode dominated by in-phase oscillations of the two nanodisk dipoles and a low energy mode dominated by antiphase oscillations. Note that the reason why the antiphase mode is so prominent in the scattering spectra is that the nanodisk sizes are different (the volume of the top disk in a dimer is only  $\sim 50\%$  of the volume of bottom one), which means that the net dipole moment associated with the mode does not vanish. As mentioned in the introduction, the low energy mode exhibits a magnetic character because the antiphase dipole oscillation corresponds to a pseudocurrent loop, or magnetic dipole, that causes a strong magnetic field enhancement in the dielectric spacer layer (see Supporting Information).<sup>11</sup> A comparison of the spectra for  $s = 10$  and 20 nm shows that the antiphase mode shifts to lower energy for smaller spacing and stronger coupling, as is expected from basic plasmon hybridization arguments.<sup>32</sup> One may also note that the antiphase mode exhibits a distinct asymmetric Fano shape. This effect is caused by destructive interference with the in-phase mode and the asymmetry is therefore most pronounced when the two modes overlap, that is, for larger spacing (see Figure S2 in the Supporting Information). Overall, the spectra are in excellent agreement with previously published results.<sup>9–11,32</sup>

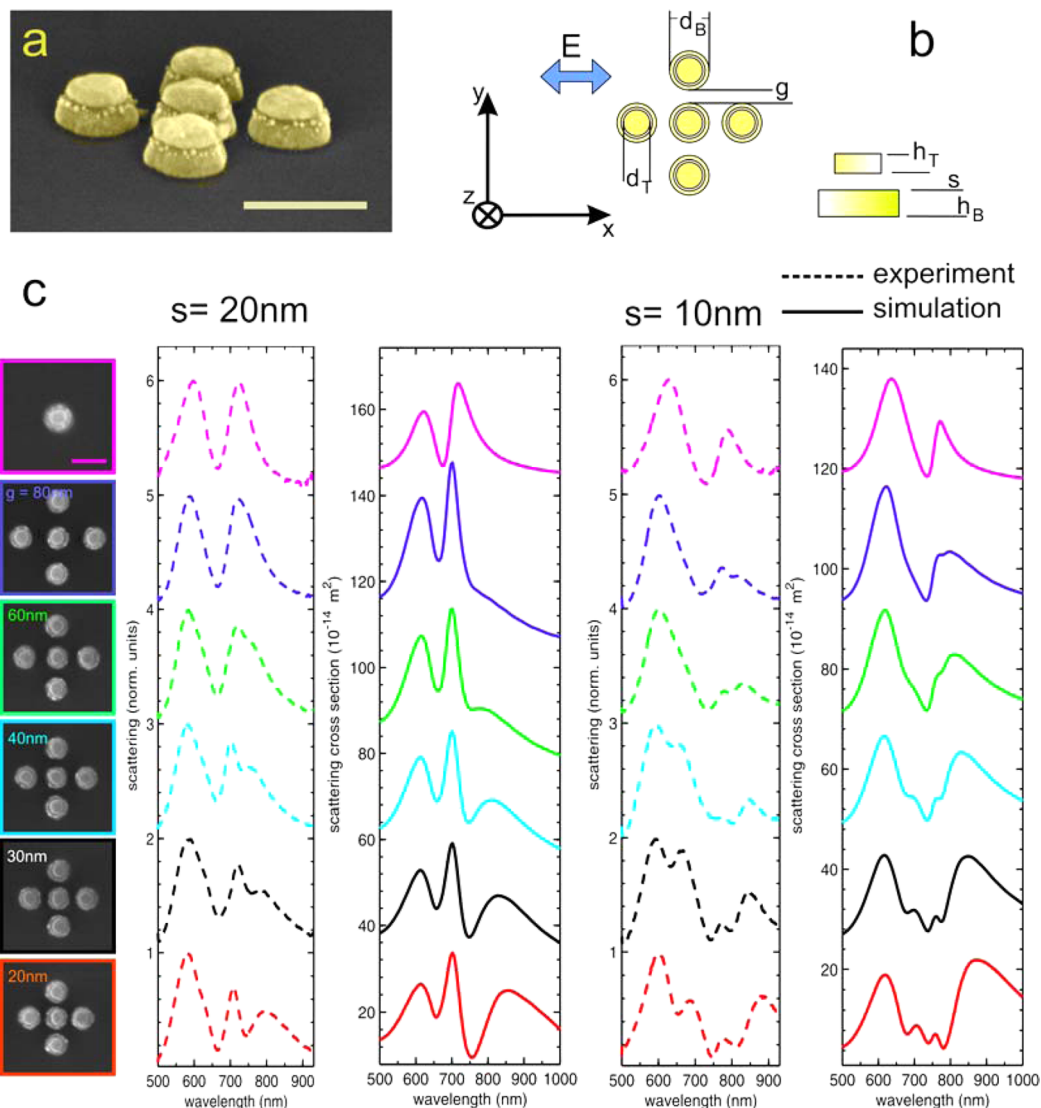


**Figure 2.** (a) Tilted SEM image of an MIM pentamer (scale bar 200 nm). (b) A sketch of the simulated system with the nomenclature used in the text. Each dimer is constructed from two cylindrical gold nanodisks with similar aspect ratio ( $d/h$ ). The incident plane wave enters from above and is polarized along  $x$ . (c) Representative experimental dark-field spectra (dashed lines) and simulated scattering spectra (continuous lines) of individual MIM pentamers for different in-plane gap distances  $g$  and for the two investigated spacer thicknesses,  $s = 20$  and  $10\text{ nm}$ , together with single dimer spectra for comparison. The color-coding links the spectra to the SEM images shown in the left column.

In order to analyze the MIM pentamer spectra, it is useful to first briefly consider the modes of a pentamer built from homogeneous nanodisks. This structure has  $D_{4h}$  symmetry and 10 in-plane dipole degrees-of-freedom. The hybridized modes of which three  $E_u$  symmetry modes are dipole active can be analyzed in terms of symmetry adapted coordinates analogous to the vibrations of a planar molecule of the same symmetry (for example  $\text{PtCl}_4^{2-}$ ).<sup>33,34</sup> However, a determination of the exact normal modes, which are linear combinations of the symmetry adapted coordinates, requires a detailed knowledge of the interparticle interactions, and these are much more complicated than for the isolated MIM dimer. The analysis is further complicated by the fact that the overall in-plane dimension of an oligomer is not negligible compared to the incident wavelength, which means that field retardation effects can be pronounced, and that the gap distances we consider are small compared to the nanodisk diameters, which means that multipolar interactions becomes important. Nevertheless, In Figure 1b, we have indicated the dipole oscillation patterns that

are most pronounced according to the electrodynamic simulations. The spectrum is dominated by a broad super-radiant mode in which the three central nanodisks that are oriented parallel to the incident field oscillate in phase. The mode is strongly redshifted compared to the dipole resonance of a single disk because of the attractive charge interaction in the gap between the particles. A second mode dominated by in-phase oscillations of the two remaining particles occurs at short wavelengths. The frequency of this mode is slightly blueshifted compared to the single disk resonance because the interparticle interactions are weakly repulsive. The spectral region between the two modes exhibit a deep asymmetric dip because the dipole oscillations of the two modes are then in antiphase, thus diminishing the total resulting dipole moment of the pentamer.

The MIM pentamer spectra in Figure 2c present multiple resonances and a complex spectral behavior, which is, however, semiquantitatively reproduced by the simulations. For large in-plane gaps  $g$ , the scattering spectra are similar to those of the isolated MIM dimers but additional features appear at longer

wavelengths when the gap is decreased. In particular, for the most strongly coupled case,  $s = 10$  nm and  $g = 20$  nm, a large dark window with smaller modulations is produced. We will later argue that this is a signature of quasi-broadband artificial magnetism.

One may expect that the combination of two basic systems that each exhibits two scattering peaks, as is the case with the 2D pentamer and the isolated MIM dimer, would always result in a composite spectrum with four peaks. This is indeed the case for the  $s = 10$  nm,  $g = 20$  nm MIM pentamer (Figure 2c bottom right). However, the scattering spectra for  $s = 20$  nm are quite different, suggesting more complicated relations. Before turning to the  $s = 10$  nm case, which is most interesting from an optical magnetism perspective, we will try to gain further insight in the spectroscopic properties of the system. For this purpose, we simulated scattering and absorption spectra for variable vertical separation  $s$  but a fixed in-plane gap  $g = 20$  nm, as shown in Figure 3. A number of different

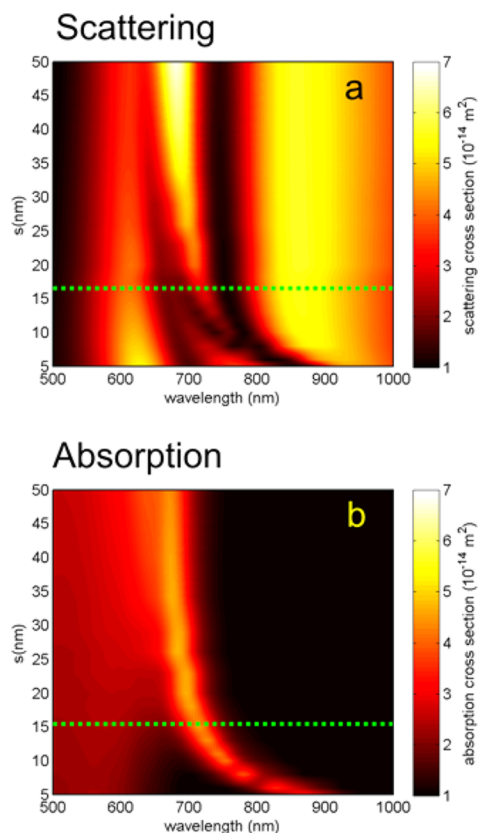


**Figure 3.** Simulated scattering (a) and absorption (b) spectra as a function of the spacing  $s$  for a MIM Fano oligomer with  $g = 20$  nm. Note the rapid dispersion of the magnetic mode and its interference with the super-radiant continuum for small separations. The horizontal dashed line is used as a guideline to mark the transition between weak and strong coupling.

resonances and Fano interferences can be identified. For the largest vertical distance,  $s = 50$  nm, the scattering spectrum is characterized by three features, a broad (super-radiant) background, a single dip ( $\lambda = 760$  nm), and a rather narrow peak ( $\sim 670$  nm), which also dominates the absorption spectrum. For intermediate distances,  $s \approx 20\text{--}40$  nm, the narrow peak begins to redshift and it develops a Fano shape with an antiresonance on its short-wavelength flank. We define

this as the weak vertically coupled (VC) regime. However, for even smaller separations  $s \approx 5\text{--}10$  nm, which we define as the strong VC regime, this new Fano interference rapidly redshifts and splits up such that an additional dip appears in the scattering spectrum. In contrast, the corresponding absorption spectra present a distinct peak in the same spectral region. To interpret these changes, we need to analyze the relative interparticle interaction strengths in the system. As a rule-of-thumb, we assume that dipole-dipole coupling between plasmonic particles is strong if the surface-to-surface distance is small compared to the particle radii.<sup>35</sup> There are three important interactions in the system: the vertical interaction, determined by the ratio between  $s$  and a characteristic vertical radius given approximately by  $R_V = (h_B + h_T)/4 \approx 15$  nm; the in-plane interaction between the bottom disks, given by  $g_B = 20$  nm and  $R_B = d_B/2 \approx 65$  nm; and the in-plane interaction between the top disks, given by  $R_T = d_T/2 \approx 42.5$  nm and  $g_T = g_B + d_B - d_T \approx 65$  nm. The spectra in Figure 3 are all characterized by  $g_B < R_B$  and  $g_T > R_T$ , that is, the bottom disks are strongly coupled but the horizontal interaction between the top disks is weak and can be neglected in a first approximation. This implies that the spectrum can be thought of as due to two essentially independent contributions for large vertical separations ( $s \gg R_V$ ): a strongly coupled pentamer, contributing with a broad super-radiant background and distinct Fano dip (Figure 1b), and five isolated disks contributing with one distinct peak. This is precisely what is observed for  $s = 50$  nm in Figure 3. When the vertical distance is decreased into the weak VC regime, the resonance of the top disk starts to interfere with the super-radiant background, causing a second dip at about 650 nm, but the interaction is not yet strong enough to induce a distinct antiphase magnetic mode. This only happens when one approaches  $s = R_V = 15$  nm, when a new magnetic dip appears and rapidly disperses toward longer wavelengths, similar to what is observed for the isolated MIM dimer (Supporting Information Figure S2). It is interesting to note that the magnetic mode manifests itself as a distinct peak in absorption but as a dip in scattering for  $s < R_V$ , indicating that it now behaves like a true “dark mode”, that is, it sucks radiative energy from the super-radiant continuum (causing a dip in the scattering spectrum) and dissipates this energy as heat (causing a peak in the absorption spectrum). Thus, the strongly coupled MIM pentamer exhibits an exotic behavior for which scattering and absorption are surprisingly different. In particular, the appearance and dispersion of the magnetic MIM mode, and its overlap with the two other Fano antiresonances, results in a “dark region” as wide as  $\sim 150$  nm with an intricate fine-structure reflecting the complex couplings in the system.

We now turn to the optical magnetism effects for small vertical separations (see Figure S5 in Supporting Information for the weak VC case). Simulated spectra and corresponding near-field plots are shown in Figure 4. For clarity, we show near-fields only for a few selected wavelengths, as indicated in Figure 4a. Figure 4c shows electric fields in horizontal cuts through the top and bottom disks together with the magnetic field-enhancement in the dielectric spacer layer. The electric-field enhancement distributions and field orientations are overall good agreement with the discussion above. The short wavelength resonance at 613 nm (position 1) corresponds to the in-phase excitation of the vertical MIM dimers. At position 2, only the top disks are efficiently excited but the particles in the central row have a  $\pi$ -phase offset, rendering the mode

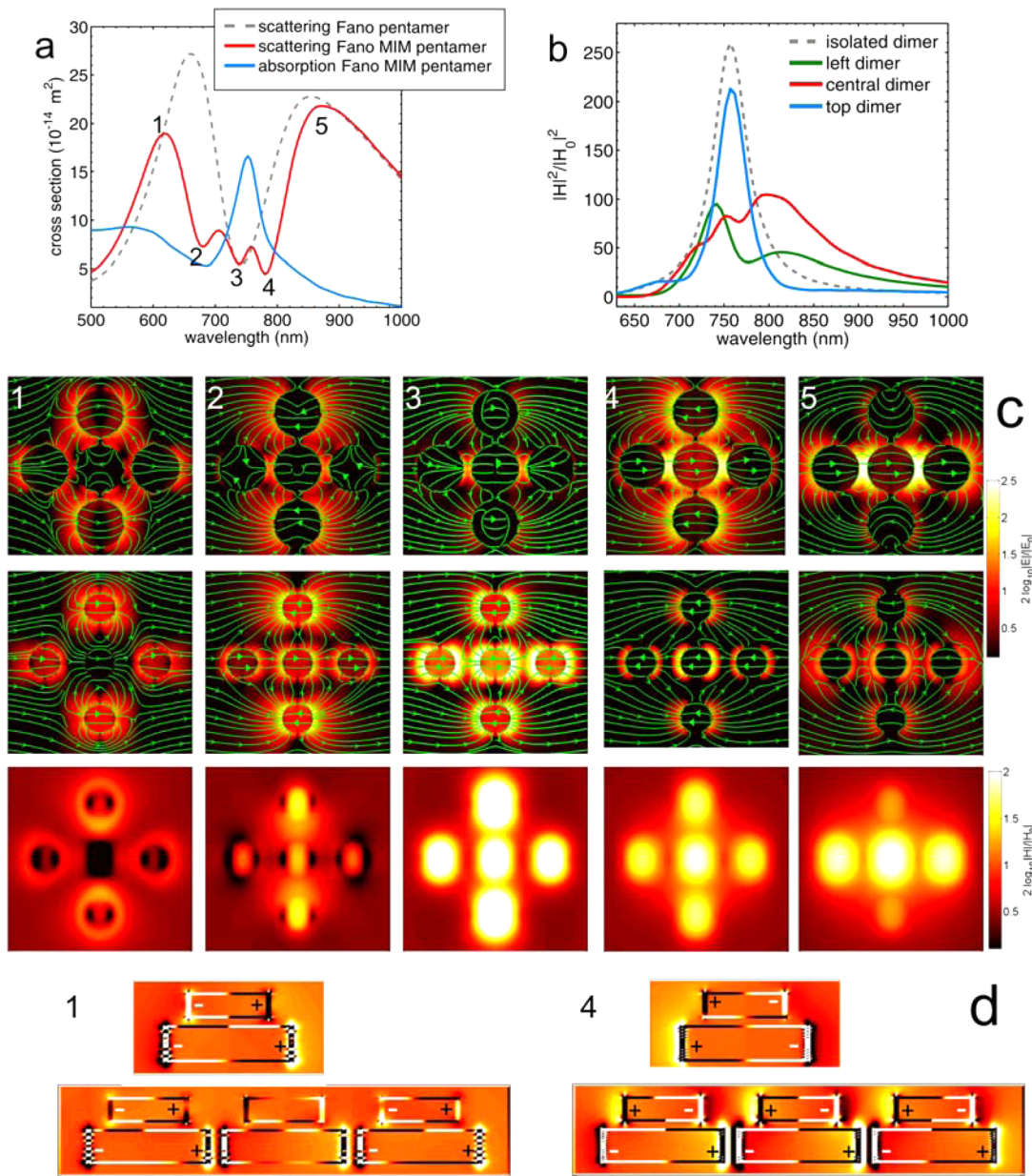


**Figure 4.** (a) Simulated spectral response of a MIM pentamer with  $s = 10 \text{ nm}$  and  $g = 20 \text{ nm}$ . The scattering of standard Fano pentamer having the same dimension of the bottom particles is also plotted. (b) Calculated magnetic field at the center of the dielectric spacer for  $s = 10 \text{ nm}$  for the different vertical dimers in the MIM pentamer. As a comparison, the magnetic enhancement for an isolated dimer is also shown. The incident light is polarized along  $x$ . Because of the strong in-plane coupling between the bottom disks, the system exhibits optical magnetism in a broad spectral region. (c) The lower images show the electric field intensity at the center of the bottom disk (first row), top disk (second row), and magnetic field in the dielectric spacer at the wavelengths indicated by 1 to 5 in *a*. The electric field lines are also indicated. (d) Vertical cross section of the simulated charge plots for the MIM dimer for the top dimer and across the central row at the wavelength positions 1 and 4. Whenever the charges oscillate in antiphase a magnetic field is generated within the dielectric spacer.

dark.<sup>36</sup> This first scattering dip is related to a dark-state induced by the phase relation between the top particles, but no strong enhancement effect is obtained as  $g_T > R_T$ . All the features at longer wavelengths can be explained by the presence of a broad super-radiant continuum, generated by the three bottom particles in the central row, superimposed with multiple dips, attributed to various dark states. These dark states are characterized by a vanishing net dipole moment of the whole structure caused by the antiphase charge oscillations of the bottom and top particles. However, it is important to note that the spectral properties are influenced by several overlapping

broad modes of varying amplitude and relative phase at a given wavelength. It is therefore difficult to associate particular features in the spectra with specific normal modes of the system.

The magnitude of the magnetic field enhancement within the spacer, shown in the bottom row of Figure 4c, is a measure of the strength the virtual current loop, or magnetic dipole, formed by the antiphase electric dipole oscillations of the top and bottom disks (see the charge plots in Figure 4d). The optical magnetism is thus driven by the exciting electric field. Because the incident field is polarized along the  $x$ -direction,

298 different behaviors are found for the left, top, and central MIM  
 299 dimers. Figure 4b compares magnetic enhancement spectra for  
 300 these three inequivalent sites. While the enhancement spectrum  
 301 of the top dimer is spectroscopically similar to that of an  
 302 isolated dimer, the left and central dimers exhibits a optical  
 303 magnetism response that is broader by a factor of 2–3 in fwhm  
 304 and that extends well outside the dark spectral region. The  
 305 reason for this behavior is that the three central dimers are  
 306 aligned with the polarization and therefore dominate the super-  
 307 radiance effect, which is the basic origin behind the broadening.  
 308 Thus, the optical magnetism originates in vertical interactions  
 309 alone, but it is rendered quasi-broadband by in-plane  
 310 interactions causing super-radiance and enhanced radiative  
 311 decay.

312 The system presented here is interesting for several reasons.  
 313 Compared with other magnetic Fano structures,<sup>14</sup> the proposed  
 314 elements could be scaled-up rather easily by standard  
 315 lithographic methods to realize a complete magnetoelectric  
 316 metamaterial with significantly broader optical magnetism  
 317 response. Additionally, the different orthogonal electric and  
 318 magnetic components are excited efficiently, which suggests  
 319 strong directionality in the far field,<sup>18,21,37,38</sup> as recently  
 320 proposed by Yang et al.,<sup>18</sup> who theoretically analyzed a system  
 321 similar to the one investigated here. We revealed that coupling  
 322 between particles produce extremely rich scattering spectra  
 323 with the existence of multiple subradiant states as a signature of  
 324 the broadband magnetism. The large subradiant dark window  
 325 realized in the strong VC regime might also be used to control  
 326 the radiative properties of molecules or quantum dots  
 327 interfaced to the nanostructure.<sup>39</sup> Finally, we have demon-  
 328 strated here a simple route to achieve multiple Fano resonances  
 329 at visible wavelength by creating 3D structures.

330 In conclusion, we have experimentally realized a 3D  
 331 plasmonic pentamer constructed from MIM dimer particles.  
 332 Each MIM dimer acts as a magnetic dipole and the in-plane  
 333 interactions within the oligomer significantly broadens their  
 334 magnetic response. We found that the system exhibits multiple  
 335 Fano resonances, a broad spectral band of “dark modes” and an  
 336 unusually contrasting absorption and scattering behavior. The  
 337 work suggests that new and exciting spectroscopic effects can  
 338 be expected in other 3D plasmonic geometries that combine  
 339 strong vertical and lateral interactions, for example, bow-tie<sup>40</sup>  
 340 antennas,<sup>40</sup> split ring resonators,<sup>41</sup> or more exotic designs<sup>42</sup>  
 341 built from MIM units.

## 342 ■ ASSOCIATED CONTENT

### 343 ■ Supporting Information

344 Full experimental and simulation details of the results presented  
 345 in the manuscript. Spectral optical response of the isolated disk  
 346 and of the vertical dimers for different *s* spacing. Standard Fano  
 347 pentamer scattering and discussion on the weak VC regimes.  
 348 This material is available free of charge via the Internet at  
 349 <http://pubs.acs.org>.

## 350 ■ AUTHOR INFORMATION

### 351 Corresponding Authors

352 \*E-mail: ruggero.verre@chalmers.se.

353 \*E-mail: mikael.kall@chalmers.se.

### 354 Notes

355 The authors declare no competing financial interest.

## ■ ACKNOWLEDGMENTS

We would like to thank Tomasz J. Antosiewicz, Kristof 357  
 Lodewijks, Mikael Svedendahl, and Dan Csontos for 358  
 stimulating suggestions and discussions. This work was 359  
 supported by the Knut and Alice Wallenberg Foundation. 360

## ■ REFERENCES

- (1) Zhou, W.; Dridi, M.; Suh, J. Y.; Kim, C. H.; Co, D. T.; Wasielewski, M. R.; Schatz, G. C.; Odom, T. W. *Nat. Nanotechnol.* **2013**, *8*, 506–511.
- (2) Xu, H.; Bjerneld, E. J.; Käll, M.; Börjesson, L. *Phys. Rev. Lett.* **1999**, *83*, 4357–4360.
- (3) Polman, A.; Atwater, H. A. *Nat. Mater.* **2012**, *11*, 174–177.
- (4) Christopher, P.; Xin, H.; Linic, S. *Nat. Chem.* **2011**, *3*, 467–472.
- (5) Fan, P.; Colombo, C.; Huang, K. C. Y.; Krogstrup, P.; Nygård, J.; Fontcuberta i Morral, A.; Brongersma, M. L. *Nano Lett.* **2012**, *12*, 370 4943–4947.
- (6) Knight, M. W.; Sobhani, H.; Nordlander, P.; Halas, N. J. *Science* **2011**, *332*, 702–704.
- (7) Maier, S. A. *Plasmonics: Fundamentals and Applications*; Springer: Berlin, 2007.
- (8) McMahon, J. M.; Gray, S. K.; Schatz, G. C. *Nano Lett.* **2010**, *10*, 376 3473–3481.
- (9) Dmitriev, A.; Pakizeh, T.; Kall, M.; Sutherland, D. S. *Small* **2007**, *3*, 294–299.
- (10) Pakizeh, T.; Abrishamian, M. S.; Granpayeh, N.; Dmitriev, A.; Kall, M. *Opt. Express* **2006**, *14*, 8240–8246.
- (11) Pakizeh, T.; Dmitriev, A.; Abrishamian, M. S.; Granpayeh, N.; Kall, M. J. *Opt. Soc. Am. B* **2008**, *25*, 659–667.
- (12) Kuznetsov, A. I.; Miroshnichenko, A. E.; Hsing Fu, Y.; Viswanathan, V.; Rahmani, M.; Valuckas, V.; Ying Pan, Z.; Kivshar, Y.; Pickard, D. S.; Luk'yanchuk, B. *Nat. Commun.* **2014**, *5*, 1–8.
- (13) Liu, N.; Kaiser, S.; Giessen, H. *Adv. Mater.* **2008**, *20*, 4521–4525.
- (14) Shafiei, F.; Monticone, F.; Le, K. Q.; Liu, X. X.; Hartseld, T.; Alu, A.; Li, X. Q. *Nat. Nanotechnol.* **2013**, *8*, 95–99.
- (15) Sheikholeslami, S. N.; Garcia-Etxarri, A.; Dionne, J. A. *Nano Lett.* **2011**, *11*, 3927–3934.
- (16) Nazir, A.; Panaro, S.; Proietti Zaccaria, R.; Liberale, C.; De Angelis, F.; Toma, A. *Nano Lett.* **2014**, *14*, 3166–3171.
- (17) Liu, H.; Leong, E. S. P.; Wang, Z.; Si, G.; Zheng, L.; Liu, Y. J.; Soci, C. *Adv. Opt. Mater.* **2013**, *1*, 978–983.
- (18) Yang, J.; Rahmani, M.; Teng, J. H.; Hong, M. H. *Opt. Mater. Express* **2012**, *2*, 1407–1415.
- (19) Lorente-Crespo, M.; Wang, L.; Ortuño, R.; García-Meca, C.; Ekinci, Y.; Martínez, A. *Nano Lett.* **2013**, *13*, 2654–2661.
- (20) Miroshnichenko, A. E.; Kivshar, Y. S. *Nano Lett.* **2012**, *12*, 6459–6463.
- (21) Wang, J. Q.; Fan, C. Z.; He, J. N.; Ding, P.; Liang, E. J.; Xue, Q. *Z. Opt. Express* **2013**, *21*, 2236–2244.
- (22) García-Meca, C.; Hurtado, J.; Martí, J.; Martínez, A.; Dickson, W.; Zayats, A. V. *Phys. Rev. Lett.* **2011**, *106*, 067402.
- (23) Pendry, J. B.; Holden, A. J.; Robbins, D. J.; Stewart, W. J. *IEEE Trans. Microwave* **1999**, *47*, 2075–2084.
- (24) Hentschel, M.; Saliba, M.; Vogelgesang, R.; Giessen, H.; Alivisatos, A. P.; Liu, N. *Nano Lett.* **2010**, *10*, 2721–2726.
- (25) Hao, F.; Sonnenfeld, Y.; Dorpe, P. V.; Maier, S. A.; Halas, N. J.; Nordlander, P. *Nano Lett.* **2008**, *8*, 3983–3988.
- (26) Chang, W.-S.; Lassiter, J. B.; Swanglap, P.; Sobhani, H.; Khatua, S.; Nordlander, P.; Halas, N. J.; Link, S. *Nano Lett.* **2012**, *12*, 4977–4982.
- (27) Gallinet, B.; Martin, O. J. F. *ACS Nano* **2013**, *7*, 6978–6987.
- (28) Ye, J.; Wen, F.; Sobhani, H.; Lassiter, J. B.; Dorpe, P. V.; Nordlander, P.; Halas, N. J. *Nano Lett.* **2012**, *12*, 1660–1667.
- (29) Thyagarajan, K.; Butet, J.; Martin, O. J. F. *Nano Lett.* **2013**, *13*, 1847–1851.
- (30) Liu, N.; Mukherjee, S.; Bao, K.; Brown, L. V.; Dorfmuller, J.; Nordlander, P.; Halas, N. J. *Nano Lett.* **2012**, *12*, 364–369.

- 423 (31) Liu, N.; Mukherjee, S.; Bao, K.; Li, Y.; Brown, L. V.;  
424 Nordlander, P.; Halas, N. J. *ACS Nano* **2012**, *6*, 5482–5488.  
425 (32) Frederiksen, M.; Bochenkov, V. E.; Ogaki, R.; Sutherland, D. S.  
426 *Nano Lett.* **2013**, *13*, 6033–6039.  
427 (33) Hopkins, B.; Poddubny, A. N.; Miroshnichenko, A. E.; Kivshar,  
428 Y. S. *Phys. Rev. A* **2013**, *88*, 053819.  
429 (34) Alegret, J.; Rindzevicius, T.; Pakizeh, T.; Alaverdyan, Y.;  
430 Gunnarsson, L.; Käll, M. *J. Phys. Chem. C* **2008**, *112*, 14313–14317.  
431 (35) Gunnarsson, L.; Rindzevicius, T.; Prikulis, J.; Kasemo, B.; Käll,  
432 M.; Zou, S.; Schatz, G. C. *J. Phys. Chem. B* **2004**, *109*, 1079–1087.  
433 (36) Rahmani, M.; Lukiyanchuk, B.; Ng, B.; Tavakkoli, K. G. A.;  
434 Liew, Y. F.; Hong, M. H. *Opt. Express* **2011**, *19*, 4949–4956.  
435 (37) Kerker, M.; Wang, D. S.; Giles, C. L. *J. Opt. Soc. Am.* **1983**, *73*,  
436 765–767.  
437 (38) Person, S.; Jain, M.; Lapin, Z.; Sáenz, J. J.; Wicks, G.; Novotny,  
438 L. *Nano Lett.* **2013**, *13*, 1806–1809.  
439 (39) Fomenko, V.; Nesbitt, D. J. *Nano Lett.* **2007**, *8*, 287–293.  
440 (40) Hanke, T.; Cesar, J.; Knittel, V.; Trügler, A.; Hohenester, U.;  
441 Leitenstorfer, A.; Bratschitsch, R. *Nano Lett.* **2012**, *12*, 992–996.  
442 (41) Clark, A. W.; Cooper, J. M. *Adv. Mater.* **2010**, *22*, 4025–4029.  
443 (42) Yu, N.; Aieta, F.; Genevet, P.; Kats, M. A.; Gaburro, Z.; Capasso,  
444 F. *Nano Lett.* **2012**, *12*, 6328–6333.